scientific reports

Check for updates

OPEN

Preparation magnetic graphene oxide/diethylenetriamine composite for removal of methylene blue from aqueous solutions

Alireza Banaei[1], Afshin Saadat[2]✉, Roghayyeh Javadi[1] & Parinaz Pargolghasemi[1]

Graphene oxide (GO) and its derivatives have several applications in many areas such as environmental and energy materials, water treatment and biomedical technologies. Because of having various polar groups on its surface, GO is considered as an excellent adsorbent. However, for many applications such as adsorption of pollution from aqueous solutions, chemical functionalization of graphene oxide is often a necessary requirement. In the present study, a new composite from graphene oxide, diethylenetriamine (DETA) and silica coated $MnFe_2O_4$ nanoparticles (GO/DETA/$MnFe_2O_4$@SiO_2) was prepared. The structure, thermal stability and magnetic properties of the composite were studied by FT-IR, XRD, SEM, EDS, VSM and TGA spectroscopic methods. The prepared composite showed magnetic property with a saturation magnetization of 3.0 emu/g. The adsorption properties of GO/DETA/$MnFe_2O_4$@SiO_2 composite for methylene blue (MB) in aqueous solution were studied using batch method. The effects of important parameters on the surface adsorption process of MB, including pH, contact time, adsorbent dosage and initial dye concentration were investigated. The adsorption isotherm was in accordance with Langmuir model showing surface homogeneity of the adsorbent. According to the Langmuir analysis, the maximum adsorption capacity (q_m) of GO/DETA/$MnFe_2O_4$@SiO_2 composite for MB was found to be 243.91 mg/g. The kinetic studies showed that the adsorption was pseudo first-order process. In addition, the thermodynamic studies indicated the adsorption was spontaneous and endothermic process.

In recent years, the growth of industries such as textile, leather, cosmetics and printing has increased pollution caused by dyes in water environments[1]. Organic dyes due to the toxic and carcinogenic are serious hazard to human, microorganisms and the ecosystem[2]. Therefore, it is urgent and important to detect and remove these toxic components from wastewater. Many methods such as adsorption[3], electrochemical oxidation[4], photocatalytic degradation[5], ion exchange[6] and nanofiltration membranes[7] have been applied to remove dyes from wastewater. Among these methods, the adsorption process seems to be the ideal choice due to the low initial cost, easy design, suitable flexibility and high efficiency[8]. In recent years, many adsorbents such as zeolites[9], activated carbon[10], alumina[11], silica gel[12], bentonite clays[13], etc. have been used for removal of toxic dyes from aqueous solutions.

One of the most important dyes used in the textile industry is methylene blue (MB), which is chemically called 3,7-bis(dimethylamino) phenazathionium chloride or tetra methylthionine chloride and is a lasting cationic dye[14]. MB is a dangerous, toxic and carcinogenic organic dye, whose release in water harms human health and the ecosystem[15]. Therefore, it is important to look for efficient methods and materials for removal of MB. A lot of different materials have been suggested as potential adsorbents for methylene blue, such as activated clay[16], graphitic materials[17], cauliflower leave[18], garlic pee[19], clay graphene oxide iron oxide[20], layered double hydroxide polymer[21], etc. However, the design and search for new adsorbents are still urgent to enhance the adsorption capacity and improve the separation rate for removal of MB from wastewater. Today, nanocomposites have a good potential to absorb MB due to their high surface area[22,23]. Nanocomposites consisting of two parts, organic and inorganic can play an effective role in improving adsorption[24].

[1]Department of Chemistry, Payame Noor University, P.O. Box 19395-3697, Tehran, Iran. [2]Department of Chemistry, Germi Branch, Islamic Azad University, Germi, Iran. ✉email: saadat@iaugermi.ac.ir

In this field, Graphene based nanocomposites have also been investigated for the removal of some organic dyes and MB from wastewater[25]. Graphene oxide (GO) has a special structure of a two-dimensional honeycomb lattice with a single layer of sp^2 carbon atoms[26,27]. Studies show that GO is an effective adsorbent towards dyes and heavy metal ions[28–31]. Its electronic and characteristic structure supply the electrostatic force and π–π stacking effect, which facilitate and contribute to the adsorption process[32–35]. Furthermore, GO is composed of many functional groups such as carboxyl groups, hydroxyl and epoxide, which lead to a hydrophilic and negatively charged surface. GO can be simply functionalized applying different treatments to change the functional groups for the purpose of gaining the desired surface properties. GO derivatives especially those functionalized with heteroatom have shown better performance as compared to its counter parts of graphene oxide[36,37]. In this filed, GO-calcium/alginate nanocomposite was synthesized and used to adsorb MB by Li et al., and the adsorption capacity was 163.93 mg g^{-1} [38]. Fan et al. synthesized a magnetic GO-chitosan nanocomposite and used it for removal of MB from aqueous solutions. The adsorption capacity was determined to be 95.31 mg g^{-1} [39]. In another study, Dai et al. doped the synthetic polymers such as PVA (poly (vinyl alcohol)) with graphene oxide in order to increase the ability of adsorption of MB. The adsorption capacity of GO/PVA composite for MB removal was 127.5 mg g^{-1} [40].

In this study, a new composite from GO, diethylenetriamine (DETA) and silica coated $MnFe_2O_4$ nanoparticles ($GO/DETA/MnFe_2O_4@SiO_2$) was synthesized (Fig. 1). The composite prepared was applied for the removal of the MB from aqueous solution. Moreover, the effects of various parameters such as pH, adsorbent dosage, initial dye concentration and contact time on adsorption behavior were studied. Adsorption isotherms, kinetics and thermodynamic studies have been reported to account for the nature of adsorption process.

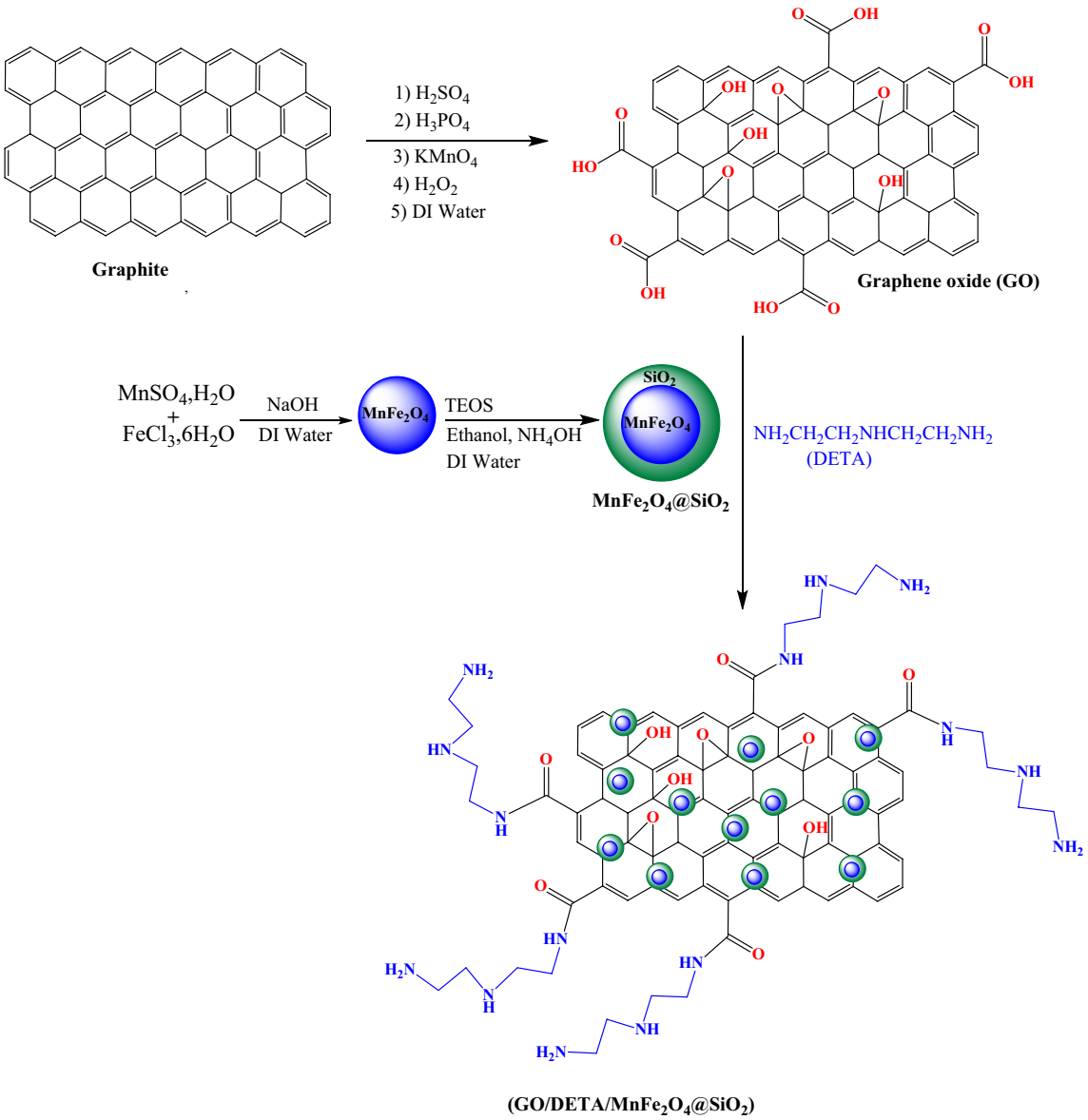

Figure 1. The synthesis route of $GO/DETA/MnFe_2O_4@SiO_2$ composite.

Results and discussion

Characterization of GO/DETA/$MnFe_2O_4$@SiO_2 composite

Infrared spectral characterization

The FT-IR spectra of synthesized compounds are demonstrated in Fig. 2. In $MnFe_2O_4$ FT-IR spectrum (Fig. 2a, blue line), a broad peak at 3428 cm^{-1} and a peak at 1627 cm^{-1} belong to stretching and bending vibration of hydroxyl (OH) groups, respectively[41]. Also, the peaks at 582 and 463 cm^{-1} are attributed to stretching vibration of Metal oxide (M–O) stretching vibrations of Mn–O and Fe–O, respectively[42]. The FT-IR spectrum of $MnFe_2O_4$@SiO_2 nanoparticles is showed in Fig. 2b (black line). As it can be observed, $MnFe_2O_4$ nanoparticles after reaction with TEOS demonstrates a new peak at 1077 cm^{-1} which is assigned to stretching vibration of Si–O–Si. Figure 2c (green line) presents the FT-IR spectrum of GO. According to the GO FT-IR spectrum, a broad peak at 3600–2500 cm^{-1} belongs to stretching vibration of hydroxyl groups (OH) and adsorbed water molecules. Furthermore, the C=O stretching vibration of carboxylic acid group demonstrates a sharp peak at 1739 cm^{-1}. Moreover, the peak at 1620 cm^{-1} is attributed to the stretching vibration mode of C=C band and the peaks at 1228 and 1052 cm^{-1} are attributed to the C–O stretching of phenolic and epoxy groups[43]. The FT-IR spectrum of GO/DETA/$MnFe_2O_4$@SiO_2 composite is showed in Fig. 2d (red line). As it can be observed, after DETA and $MnFe_2O_4$@SiO_2 modification, the peak of GO at 1739 cm^{-1} disappears indicating the reduction of C=O of carboxylic acid group because of amine functionalization. Also, new peaks appear at 1516 and 1085 cm^{-1} which belong to N–H bending and Si–O–Si stretching, respectively. Besides, in the FT-IR spectrum of GO the peak at 1381 cm^{-1} is attributed to C–OH band and due to ammination process its intensity has been decreased[44].

XRD analysis

X-ray diffraction of $MnFe_2O_4$ nanoparticles, GO and GO/DETA/$MnFe_2O_4$@SiO_2 composite are demonstrated in Fig. 3. For the $MnFe_2O_4$ nanoparticles, XRD patterns (Fig. 3a) show the typical peaks $2\theta = 30.20°$, 35.45°, 43.25°, 53.50°, 57.15° and 63.40°, which are in agreement with the referenced data for $MnFe_2O_4$ nanoparticles[45]. Figure 3b presents XRD patterns of GO. The strong diffraction peak at $2\theta = 10.49°$ shows that interlayer spacing of GO based on the Bragg equation is 8.4 Å. Figure 3c shows XRD patterns of GO/DETA/$MnFe_2O_4$@SiO_2 composite. The XRD pattern of GO/DETA/$MnFe_2O_4$@SiO_2 composite includes the $MnFe_2O_4$ peaks with a peak at $2\theta = 9.8°$ which is attributed to GO. The average particles size of GO/DETA/$MnFe_2O_4$@SiO_2 composite is calculated via Debye–Scherer equation:

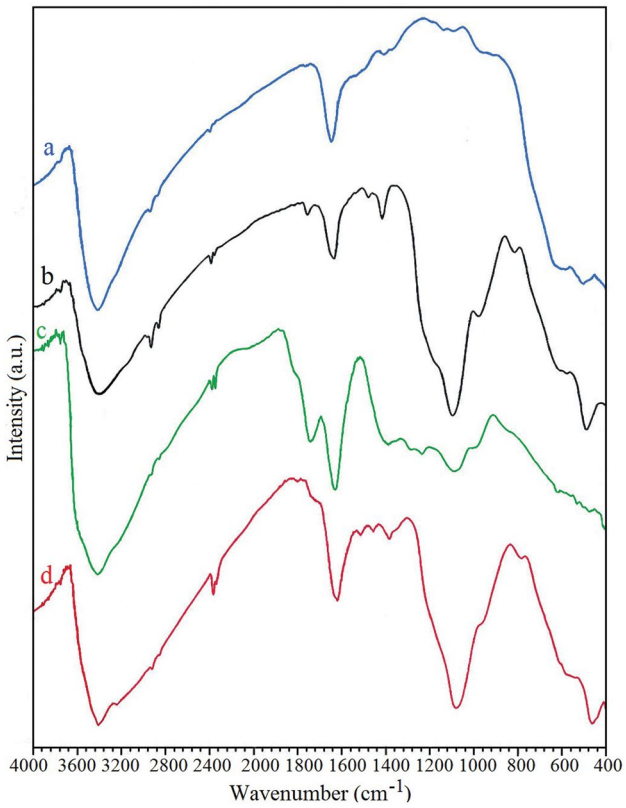

Figure 2. FT-IR spectra of (**a**) $MnFe_2O_4$, (**b**) $MnFe_2O_4$@SiO_2, (**c**) GO, (**d**) GO/DETA/$MnFe_2O_4$@SiO_2 composite.

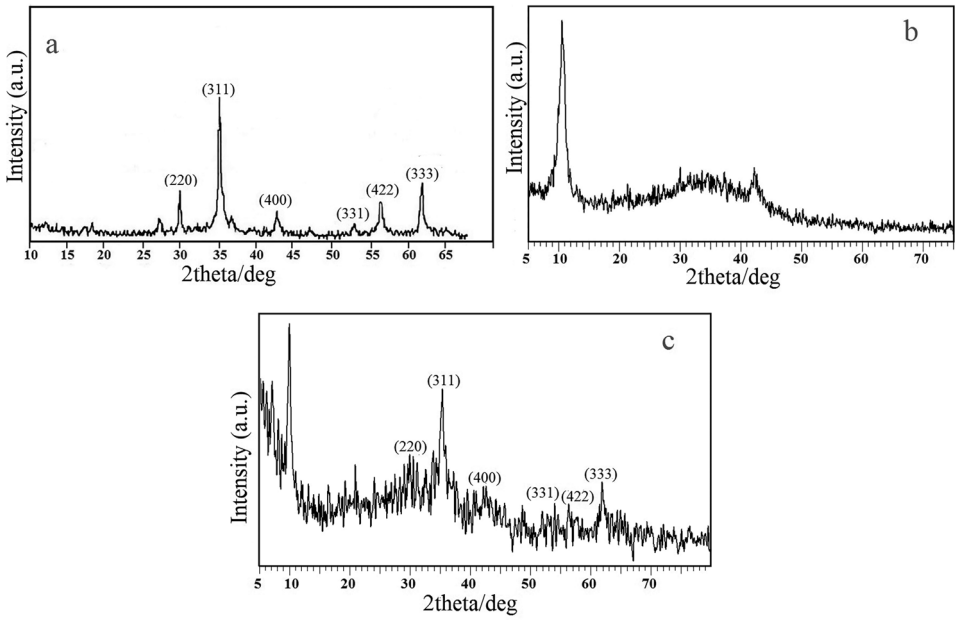

Figure 3. XRD pattern of (**a**) $MnFe_2O_4$ nanoparticles, (**b**) GO and (**c**) GO/DETA/$MnFe_2O_4$@SiO_2 composite.

$$D = \frac{K\lambda}{\beta \cos\theta}$$

where D is the average size, λ is the X-ray source wavelength (1.54 Å), β is the full width at half maximum (FWHM) of the diffraction peak and θ is the Bragg's angle.

The average particle size of the GO/DETA/$MnFe_2O_4$@SiO_2 composite is obtained based on Debye–Scherrer equation 149 nm.

SEM and EDS analysis

The particle size and surface morphology of $MnFe_2O_4$@SiO_2 and GO/DETA/$MnFe_2O_4$@SiO_2 composite were studied applying SEM technique. As illustrated in Fig. 4a, $MnFe_2O_4$@SiO_2 nanoparticles are mostly in spherical shape and have average particle size about 244 nm. Figure 4b demonstrates the SEM image of GO/DETA/$MnFe_2O_4$@SiO_2 composite. SEM confirms verify the presence of spherical $MnFe_2O_4$@SiO_2 nanoparticles on the surface of GO/DETA/$MnFe_2O_4$@SiO_2 nanocomposite. The SEM image of GO/DETA/$MnFe_2O_4$@SiO_2 composite obviously illustrates that it has created a layered structure and the spherical $MnFe_2O_4$@SiO_2 nanoparticles have the average particle size about 230 nm. The chemical composition of GO/DETA/$MnFe_2O_4$@SiO_2 composite is studied via EDS analysis. The EDS spectrum of composite is presented in Fig. 5. EDS measurement confirms that the composite contains C, N, O, Si, Mn and Fe. The EDS spectrum of GO/DETA/$MnFe_2O_4$@SiO_2 composite shows the atomic percentage of C, N, O, Si, Mn and Fe are 22.53, 10.71, 45.49, 9.01, 9.52 and 2.74, respectively.

Magnetization analysis (VSM)

The magnetic moment of the $MnFe_2O_4$, $MnFe_2O_4$@SiO_2 and GO/DETA/$MnFe_2O_4$@SiO_2 composite were calculated over a range of applied fields between 10,000 and − 10,000 Oe. Figure 6 shows magnetization curves of the

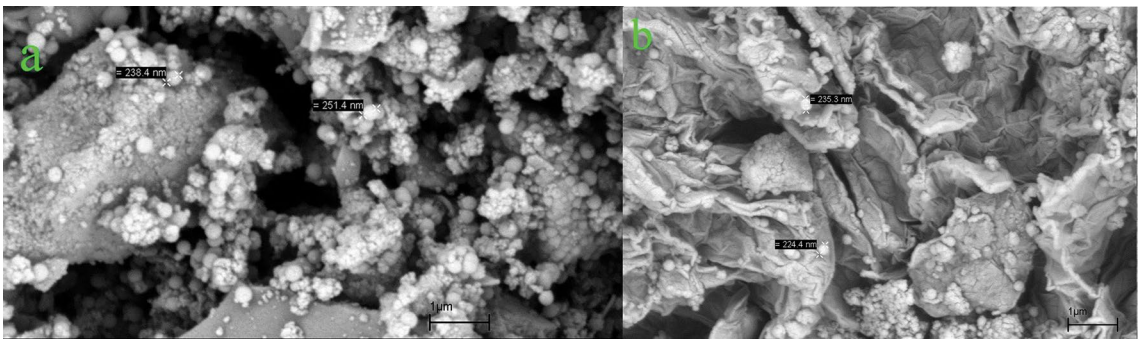

Figure 4. SEM images of (**a**) $MnFe_2O_4$@SiO_2, (**b**) GO/DETA/$MnFe_2O_4$@SiO_2 composite.

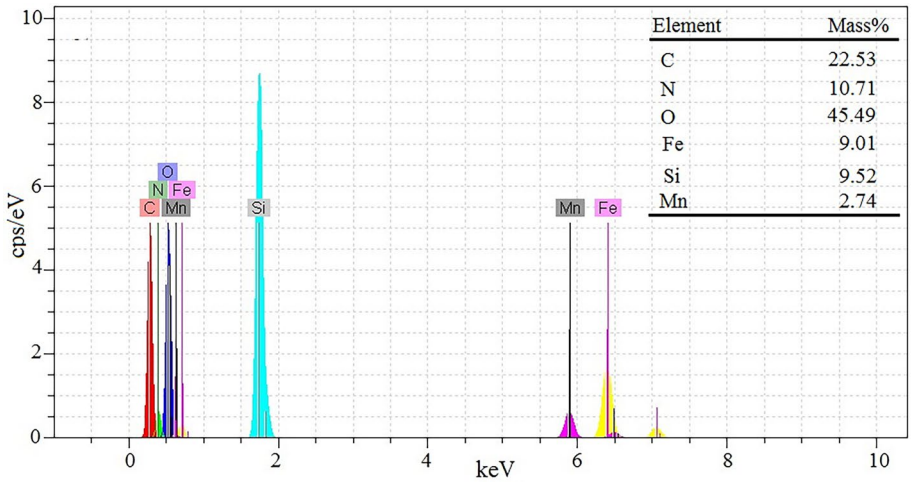

Figure 5. EDS patterns of GO/DETA/$MnFe_2O_4$@SiO_2 composite.

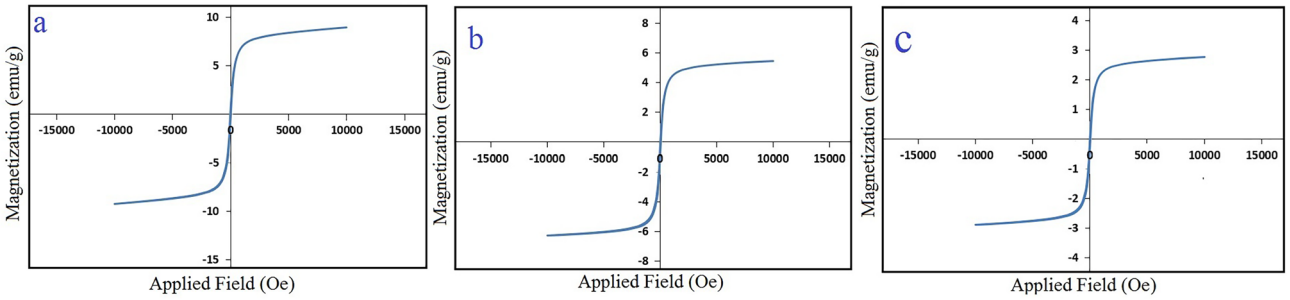

Figure 6. Magnetic hysteresis loops of (**a**) $MnFe_2O_4$, (**b**) $MnFe_2O_4$@SiO_2 and (**c**) GO/DETA/$MnFe_2O_4$@SiO_2 composite.

$MnFe_2O_4$, $MnFe_2O_4$@SiO_2 and GO/DETA/$MnFe_2O_4$@SiO_2 at room temperature. As presented, the saturation magnetization value of $MnFe_2O_4$ to GO/DETA/$MnFe_2O_4$@SiO_2 is decreased sequentially. These results confirm that, the surface of the $MnFe_2O_4$ nanoparticles are successfully coated with silica, DETA and GO. The saturation magnetization values of $MnFe_2O_4$, $MnFe_2O_4$@SiO_2 and GO/DETA/$MnFe_2O_4$@SiO_2 are 10, 6 and 3 emu/g, respectively.

TGA analysis

Thermo-gravimetric Analysis (TGA) was done to predict the thermal stability of the GO/DETA/$MnFe_2O_4$@SiO_2 composite. Figure 7 demonstrates the TGA-DTG curve of the GO/DETA/$MnFe_2O_4$@SiO_2 composite. The TGA-DTG revealed three-stage degradation pattern between 25 and 600 °C. The first stage degradation happened between 25 and 135 °C with 11.5%, which could be assigned to the release of adsorbed water in the sample[46]. The second weight loss (18.4%) within 135–250 °C can be related to the degradation of groups that contain oxygen[47]. In the third stage, in the range from 250 to 550 °C, the major weight loss occurred and was decomposed 34.7% of GO/DETA/$MnFe_2O_4$@SiO_2 composite, which can be at attributed to the decomposition of the carbon skeletons of GO and DETA[48].

Sorption studies of selected dye

Effect of adsorbent dosage

The important factor that influences adsorption processes is adsorbent dosage since it characterizes the capacity of adsorbent for a given initial concentration of dye solution[49]. In our work, the effect of adsorbent dosage on adsorption removal of MB was investigated with sorbent amounts in the range 0–30 mg in the adsorption systems containing 40 mL of 100 mg/l solution of dye at 25 °C for 10 min. Figure 8 displays the effect of adsorbent dosage on the percentage removal of MB. As shown, the percentage removal of MB increased from 0 to 89% with increasing GO/DETA/$MnFe_2O_4$@SiO_2 composite. This phenomenon can be related to the increasing of the surface area of the adsorbent and availability of more adsorption sites. Based on the results in Fig. 8, an optimum adsorbent dosage of 25 mg was selected.

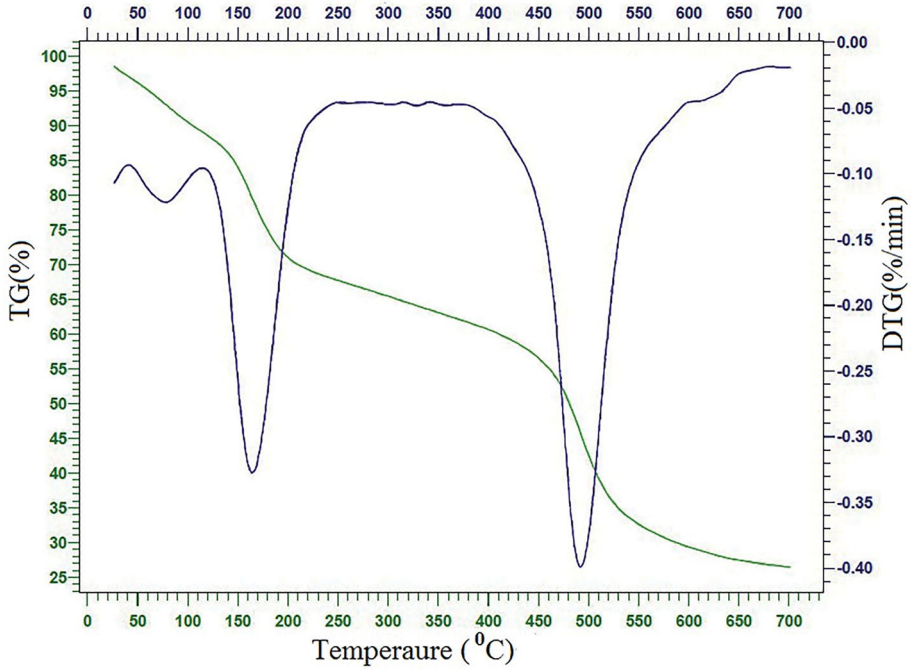

Figure 7. TGA-DTG curve of GO/DETA/$MnFe_2O_4$@SiO_2 composite.

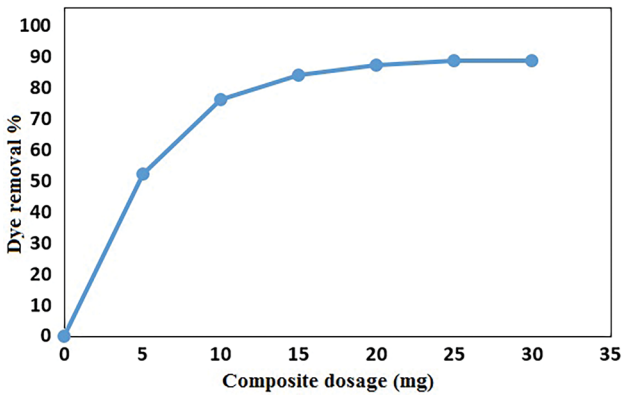

Figure 8. Effect of adsorbent dosage on removal of MB by GO/DETA/$MnFe_2O_4$@SiO_2 composite (100 mg/l, 200 rpm, 25 °C, 10 min, pH = 7).

Effect of initial dye concentration

The influence of initial dye concentration on adsorption in case of GO/DETA/$MnFe_2O_4$@SiO_2 composite was studied with different solution concentrations (30–150 mg/l) applying 25 mg of adsorbent. As it is shown in Fig. 9, the dye removal percentage is decreased with the increase of the initial dye concentration, which may be due to the decrease of enough number of active sites of GO/DETA/$MnFe_2O_4$@SiO_2 composite for binding on the dye molecules.

Effect of contact time

The effect of contact time on the adsorption of MB on GO/DETA/$MnFe_2O_4$@SiO_2 composite is demonstrated in Fig. 10. As can be seen in Fig. 10, with increasing contact time, the adsorption percentage of MB has increased rapidly in the early stages because of high availability of vacant adsorption sites. After a period of 10 min, the adsorption illustrated a steady increase.

Effect of initial pH solution

The pH of solution is an important factor due to separation of different functional groups on the adsorbent and ionization of adsorbent in solution. The effect of pH on the sorption of MB onto GO/DETA/$MnFe_2O_4$@SiO_2 composite was investigated within pH range 2–12 (Fig. 11). As it can be observed in Fig. 11 with increasing the

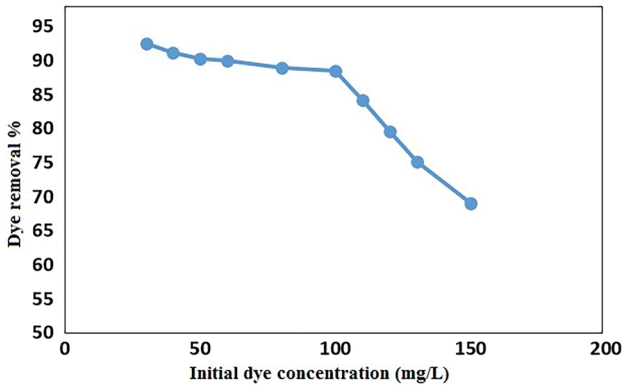

Figure 9. Effect of initial dye concentration on removal of MB by GO/DETA/$MnFe_2O_4$@SiO_2 composite (25 mg, 200 rpm, 25 °C, 10 min, pH = 7).

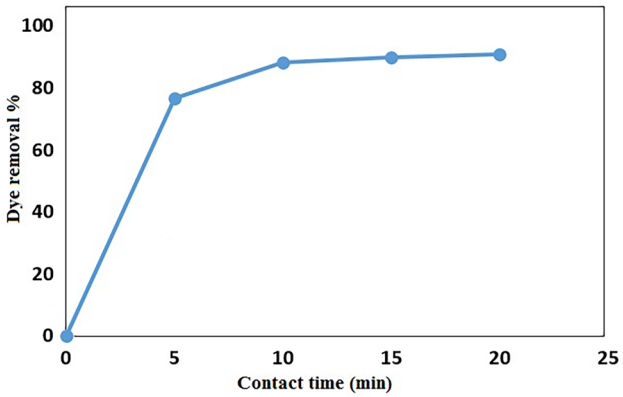

Figure 10. Effect of contact time on removal of MB by GO/DETA/$MnFe_2O_4$@SiO_2 composite (100 mg/l, 25 mg, 200 rpm, 25 °C, pH = 7).

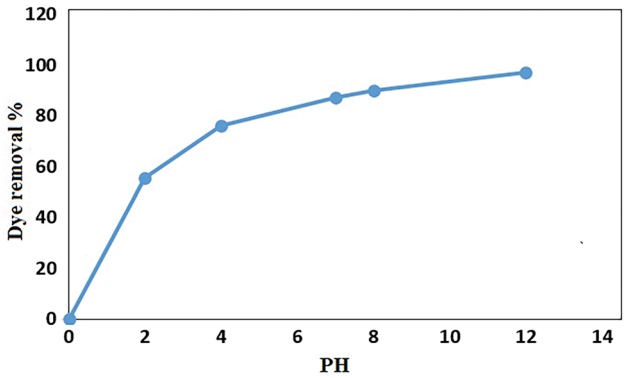

Figure 11. Effect of pH solution on removal of MB by GO/DETA/$MnFe_2O_4$@SiO_2 composite (200 rpm, 25 °C, 10 min).

pH solution, the removal of MB was increased. At higher pH, the surface has a negative charge and produces electrostatic interactions with MB cationic molecules[50].

Adsorption isotherms

One of the important parameters for study of the interaction between adsorbent and dye are adsorption isotherms[51]. In this study, Langmuir and Freundlich isotherm models were applied to gain the isotherm parameters for adsorption of MB onto GO/DETA/$MnFe_2O_4$@SiO_2 composite. One of the well-known models

to study the monolayer adsorption is Langmuir isotherm model. In this model the surface contains finite number of sites having equal activation energy of adsorption. The linear model of Langmuir isotherm is showed as follows:

$$\frac{C_e}{q_e} = \frac{1}{K_L \cdot q_m} + \frac{C_e}{q_m} \quad (1)$$

where C_e is the concentration of the dye solution at equilibrium (mg/l), q_e is the maximum amount of dye adsorbed (mg/g), q_m indicates the value of monolayer adsorption capacity and K_L is the constant value of Langmuir (mg/l). The values of K_L and q_m were obtained from the plot of (C_e/q_e) versus C_e. The Langmuir plot for the adsorption of MB onto GO/DETA/$MnFe_2O_4$@SiO_2 composite is illustrated in Fig. 12.

Freundlich isotherm model is used for reversible heterogeneous surface and is showed by the following linearized equation:

$$\text{Ln } q_e = \text{Ln } K_f + \left(\frac{1}{n}\right) \text{Ln } C_e \quad (2)$$

where K_F and n are adsorption capacity (L/mg) and intensity of adsorption, respectively. The K_F and 1/n can be calculated from the linear plot of Ln qe versus Ln Ce (Fig. 13). The 1/n values represent irreversible (1/n = 0), favorable (0 < 1/n < 1) or unfavorable (1/n > 1) condition for adsorption.

The separation factor (R_L) was determined by the following equation:

$$R_L = \frac{1}{1 + K_L \cdot C_0} \quad (3)$$

where K_L is the Langmuir constant and C_0 is the highest initial concentration of adsorbent (mg/l). The values of R_L can demonstrate the shape of the isotherm. If $R_L > 1$, the adsorption is unfavorable; if $R_L = 1$, the adsorption is linear; if $0 < R_L < 1$, the adsorption is favorable and if $R_L = 0$ the adsorption is irreversible. Table 1 shows the values of Langmuir and Freundlich parameters and the regression coefficients (R^2) of the MB onto GO/DETA/$MnFe_2O_4$@SiO_2 composite. Based on R^2 values, the experimental data were found to fit with Langmuir isotherm model for adsorbent. Also, the value of R_L lying in the range $0 < R_L < 1$ confirms the favorable condition for adsorption of MB onto GO/DETA/$MnFe_2O_4$@SiO_2 composite. Based on the result, the Langmuir model suggests

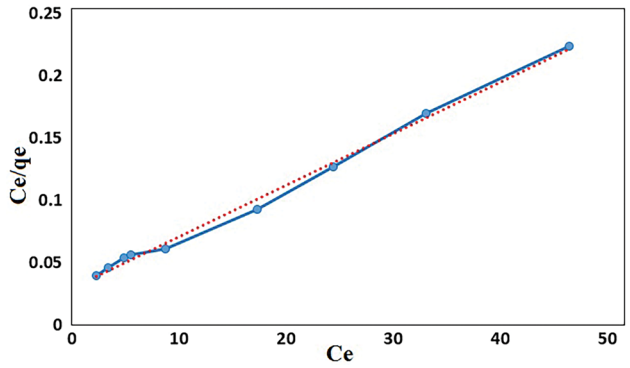

Figure 12. Langmuir plot for the adsorption of MB (200 rpm, 25 °C and pH = 7).

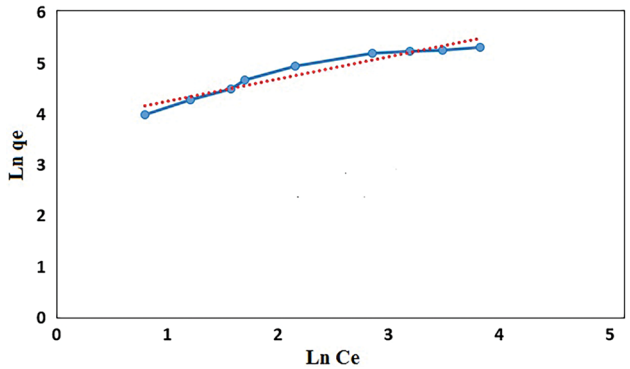

Figure 13. Freundlich plot for the adsorption of MB (200 rpm, 25 °C and pH = 7).

Langmuir isotherm parameters				Freundlich isotherm parameters		
q_m (mg/g)	K_L (L/mg)	R_L	R^2	K_F (L/mg)	n	R^2
243.91	0.136	0.068	0.9951	44.45	2.29	0.9269

Table 1. Langmuir and Freundlich isotherms parameters and correlation coefficients for the adsorption of MB onto GO/DETA/$MnFe_2O_4$@SiO_2 composite.

homogeneous surfaces of the GO/DETA/$MnFe_2O_4$@SiO_2 composite and monolayer coverage of MB onto the adsorbent. The maximum monolayer adsorption capacity (qm) was 243.91 mg/g for MB.

Kinetic model for MB adsorption

For investigating the mechanism of adsorption of MB two kinetic models: (i) pseudo-first order and (ii) pseudo-second order models have been studied. The linear form of pseudo-first-order[52] and pseudo-second-order[53] kinetic are expressed in Eqs. (4) and (5), respectively:

$$\log\left(q_e - q_t\right) = \log q_e - \frac{K_1}{2.303}t \tag{4}$$

$$\frac{t}{q_t} = \frac{1}{K_2 q_e^2} + \frac{t}{q_e} \tag{5}$$

where q_e and q_t (mg/g) is the amount of dye adsorbed at equilibrium and at time t, K_1 and K_2 (min^{-1}) are the rate constants. The adsorption kinetics plots obtained for MB on GO/DETA/$MnFe_2O_4$@SiO_2 composite are demonstrated in Fig. 14. The constants obtained for pseudo-first order and pseudo-second order models are listed in Table 2. Based on the results, the pseudo-first order model fit demonstrates a higher R^2 value compared to the pseudo-second order for adsorbent. Also, the q_e value gained by calculating pseudo-first order kinetic is closer to the experimental value (177.25 mg/g).

Thermodynamics of adsorption

In order to study the thermodynamic factors such as standard enthalpy change (ΔH°), standard Gibbs free energy change ($\Delta G°$) and standard entropy change (ΔS°), adsorption studies have been done at different temperatures (285–320 K). The thermodynamic factors were examined using following equations:

$$\mathrm{Ln}K_C = -\frac{\Delta H^\circ}{RT} + \frac{\Delta S^\circ}{R} \tag{6}$$

$$\Delta G^\circ = \Delta H^\circ - T\Delta S^\circ \tag{7}$$

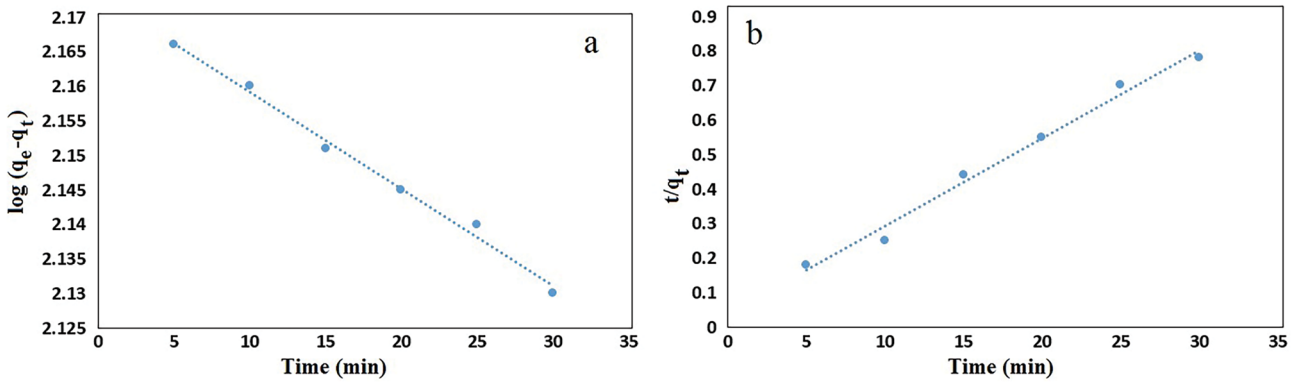

Figure 14. Pseudo-first-order (**a**) and Pseudo-Second-order (**b**) model for the removal kinetics of MB on GO/DETA/$MnFe_2O_4$@SiO_2 composite (100 mg/l, 25 °C and pH = 7).

Pseudo-first-order			Pseudo-Second-order		
q_e (mg/g)	K_1 ($\times 10^{-3}$)(min^{-1})	R^2	q_e (mg/g)	K_2 ($\times 10^{-3}$)(min^{-1})	R^2
147.91	3.22	0.9922	39.21	17.43	0.9876

Table 2. Kinetic parameters for the adsorption of MB onto GO/DETA/$MnFe_2O_4$@SiO_2 composite.

where K_C is the thermodynamic equilibrium constant, T is the solution temperature and R is the universal gas constant (8.314 J/mol K). The values of ΔH° and ΔS° were determined from slope and intercept of plot Ln K_L vs 1/T (Fig. 15). Table 3 demonstrates the values of various thermodynamic parameters for the adsorption of MB on GO/DETA/$MnFe_2O_4$@SiO_2 composite. The positive value of ΔH° indicates that the adsorption of MB on GO/DETA/$MnFe_2O_4$@SiO_2 composite is endothermic and the positive value of ΔS° suggests the increase in randomness and disorder at the adsorbent-solution interface during the adsorption of MB on GO/DETA/$MnFe_2O_4$@SiO_2 composite. Also, the negative values of ΔG° show that the adsorption of MB on GO/DETA/$MnFe_2O_4$@SiO_2 composite is spontaneous process.

Adsorption mechanism

The pH of solution plays an important role because of the separation of different functional groups on the adsorbent and ionization of adsorbent in solution. It was found that the adsorption efficiency increased with increasing pH (Fig. 11). With the increase of pH, the negative charges in the solution are increased. This could be because of the ionization of functional groups such as hydroxyl on the composite. Therefore, increasing the surface charge density raises the MB removal percentage due to the increasing electrostatic interactions between the negative charge of the composite and the positive charge of the MB (Fig. 16)[54]. As a result, the electrostatic interactions between the positive charge on nitrogen group of MB and the negative charge on oxygen group may act as the critical adsorption mechanism[55]. Also, the localized π electrons in the conjugated aromatic rings of the composite can interact by the C–C double bond of MB through π-π interaction[56]. Finally, the hydrogen bonding interactions between amine or oxygen containing groups of composite and hydrogen containing groups of MB play important role in the adsorption of MB on GO/DETA/$MnFe_2O_4$@SiO_2 composite[57] (Fig. 16).

Reusability studies

In the study of adsorption process, reusability is of great importance from the cost point of view in water treatment. To study the regeneration ability of the GO/DETA/$MnFe_2O_4$@SiO_2 composite, four cycles of MB removal were evaluated[58]. The percentage removal of MB in 0.1 M HCl solution is represented in Fig. 17. As it can be observed from Fig. 17, the MB removal percentage decreased slightly and was still 74%.

Comparison with other reported adsorbents

The adsorption capacity of GO/DETA/$MnFe_2O_4$@SiO_2 composite for removal of MB was compared with GO-based adsorbents and other adsorbents reported in the literature (Table 4). As it is shown in Table 4, the adsorption capacity of GO/DETA/$MnFe_2O_4$@SiO_2 composite is acceptable for removal of MB from aqueous solutions.

Conclusion

The GO/DETA/$MnFe_2O_4$@SiO_2 composite has been successfully prepared and characterized by FTIR, XRD, SEM, EDS, VSM and TGA techniques. The composite showed magnetic property with a saturation magnetization of 3 emu/g. It was found that the GO/DETA/$MnFe_2O_4$@SiO_2 composite was effective in adsorption of MB from aqueous solution. The effects of different parameters such as adsorbent dosage, initial drug concentration, pH and

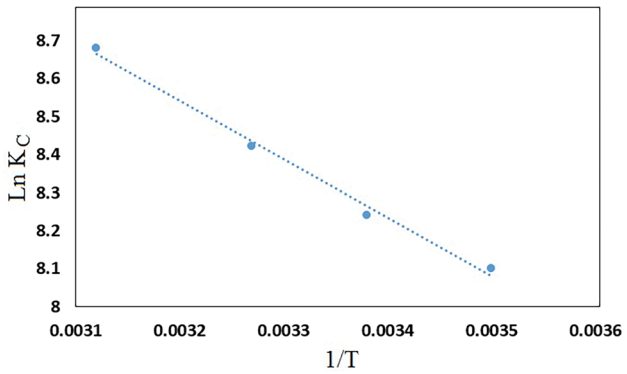

Figure 15. Thermodynamic plot for removal of MB on GO/DETA/$MnFe_2O_4$@SiO_2 composite (200 rpm, 25 °C and pH = 7).

Adsorbent	Adsorbate	ΔH° (kJ/mol)	ΔS° (kJ/mol)	ΔG° (kJ/mol)			
				285 K	295 K	305 K	320 K
GO/DETA/$MnFe_2O_4$@SiO_2	MB	12.53	0.12	− 21.67	− 22.87	− 24.07	− 25.87

Table 3. Thermodynamic parameters for the adsorption of MB on GO/DETA/$MnFe_2O_4$@SiO_2 composite.

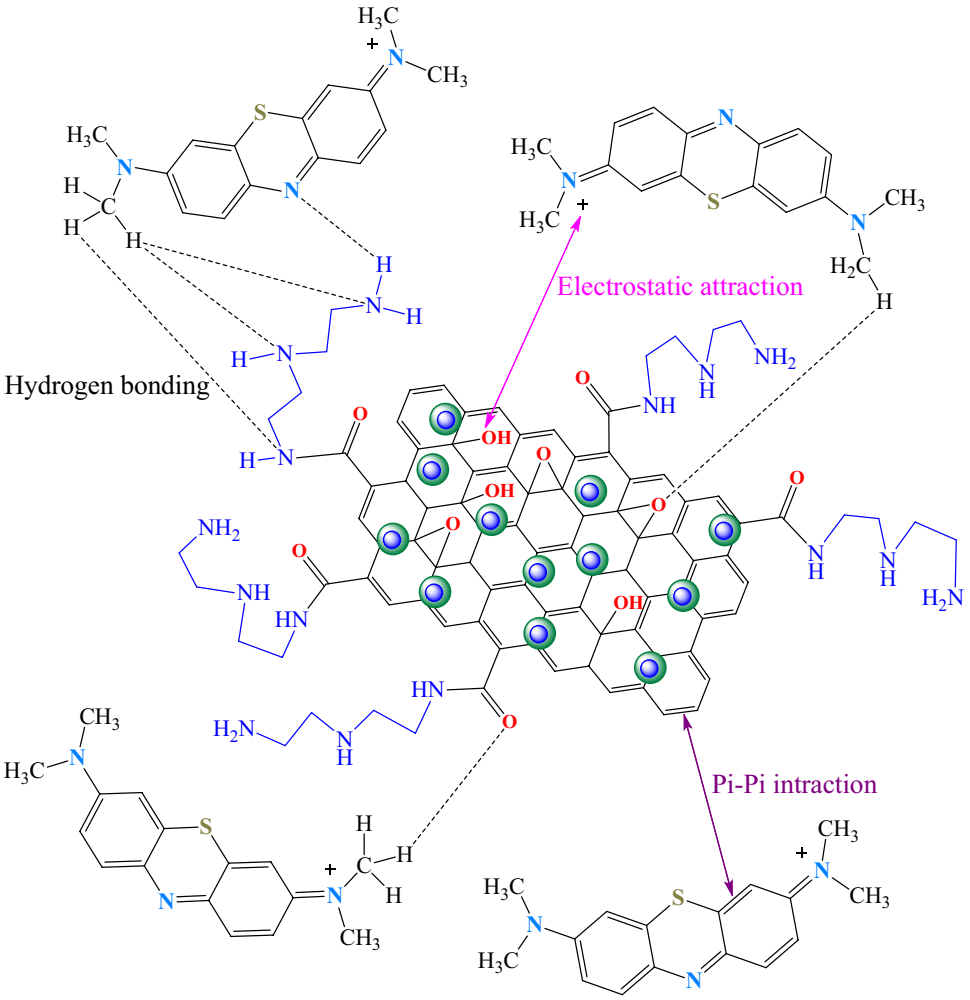

Figure 16. Different adsorption mechanisms of GO/DETA/$MnFe_2O_4$@SiO_2 composite for MB.

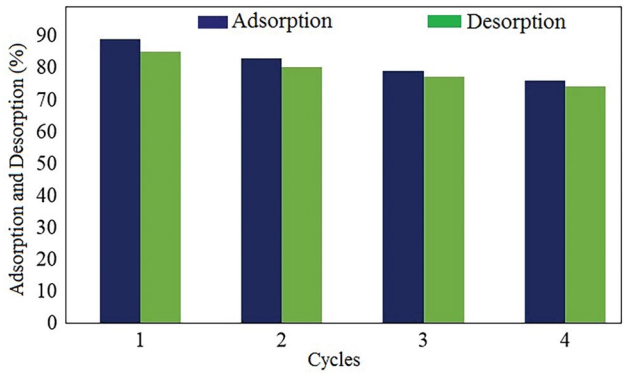

Figure 17. Regeneration studies for the adsorption–desorption of MB onto GO/DETA/$MnFe_2O_4$@SiO_2 composite.

contact time were investigated. The Langmuir isotherm model was the best model to understand the adsorption process. According to the Langmuir analysis, the maximum adsorption capacity (qm) of the adsorbent for MB was obtained to be 243.91 mg/g. Kinetic studies demonstrated that the adsorption process followed pseudo-first order model for MB. The thermodynamic study illustrated that adsorption of MB on composite was spontaneous and endothermic, which was proceeded via hydrogen bonding, electrostatic and π-π interactions.

Adsorbents	Dye	q_m (mg/g)	References
Graphene oxide/calcium alginate	MB	182	[59]
Graphene–carbon nanotube	MB	82	[60]
RCE/GO	MB	68	[61]
Pt–Co@GO	MB	90	[62]
GO/silicates	MB	90	[63]
GO-PDA-PSPSH	MB	185	[64]
GO	MB	100	[65]
Poly(AA-co-AMPS)/montmorillonite	MB	192	[66]
MgAl-layered double hydroxides	MB	102	[67]
Poly(AAc)	MB	220	[68]
Cu-Z-GO-M	MB	94.48	[69]
GO/DETA/$MnFe_2O_4$@SiO_2	MB	243.91	Present study

Table 4. Comparison of the adsorption capacity of present system with other reported systems.

Experimental

Chemicals and instrumentation

All the chemicals were purchased from Merck. Methylene blue (chemical formula = $C_{16}H_{18}ClN_3S$, Molecular weight (g/mol) = 319.85) was purchased from the Textile Factory. FT-IR spectra (Shimadzu prestige-21) were used to determine the identity of the as prepared nanocomposite. X-ray powder diffraction measurements were performed using an X-ray diffractometer (XRD) (Perkin Elmer) at ambient temperature. The surface morphology of the synthesized compounds was identified with a scanning electron microscope (LECO SEM, Michigan, USA). The elemental analysis was performed using energy-dispersive X-ray spectroscopy (EDS) on a scanning electron microscope, Mira 3-XMU model. Magnetic measurements were performed by means of the vibrating sample magnetometery method, using a VSM 7407 magnetometer, at room temperature. Thermogravimetric analysis (TGA) was performed using a Perkin Elmer thermogravimetric analyzer. UV–visible spectra in the 200–1000 nm range were obtained in DMF solvent on a Perkin Elmer Lambda 45 spectrophotometer. A Jenway model 4510 pH-meter was used for pH measurements by use of a combined electrode. An ultrasonication probe (Karl Deutsch, Germany) was used to disperse the nanoparticles in the solution.

Preparation of the GO/DETA/$MnFe_2O_4$@SiO_2 composite

Preparation of GO

GO was prepared using the reported modified method[70]. Graphite powder (2.0 g) were dissolved in a mixture of H_2SO_4 and H_3PO_4 (150:15) with stirring at 60 °C. Then, 10 g of $KMnO_4$ was added to the mixture and stirred for 12 h until its color changed to brown. Afterward, the mixture was cooled then 300 ml deionized water and 4 ml H_2O_2 (30%) was added. The mixture was centrifuged and the residue was washed with HCl (10%) followed by deionized water several times until the pH achieved neutral and dried under vacuum.

Preparation of Manganese Ferrite Nanoparticles ($MnFe_2O_4$)

$MnFe_2O_4$ NPs was prepared using the reported modified method[71]. Briefly, 0.9 g of $FeCl_3.6H_2O$ and 1.5 g of $MnSO_4{\cdot}H_2O$ were dissolved in 200 ml deionized water with stirring at 80 °C. Then, NaOH (8 M) was added slowly to the solution to raise the pH to 10. The solution was stirred under nitrogen gas at 80 °C for 3 h. Afterward, $MnFe_2O_4$ NPs precipitates was separated by a magnetic separation and then washed with deionized water and ethanol. Then, the $MnFe_2O_4$ NPs were dried at 60 °C for 24 h.

Preparation of silica-coated nanoparticles $MnFe_2O_4$@SiO_2

$MnFe_2O_4$ (6 g) was dispersed in a 100 ml of 0.1 M HCl aqueous solution. Then, solution ultrasonically agitated for 20 min. The nanoparticles isolated and washed with deionized water. Then, the nanoparticles were suspended 40 ml deionized water, 100 ml ethanol and 15 ml 28% ammonia solution and stirred for 1 h. Afterward, tetraethylorthosilicate (20 ml) in 20 ml ethanol was added to solution. This solution was stirred for 10 h at room temperature. Then, the product $MnFe_2O_4$@SiO_2 were separated by an external magnet and washed with deionized water and ethanol.

Preparation of GO/DETA/$MnFe_2O_4$@SiO_2 composite

0.5 g of GO was placed into 100 ml DMF and ultrasonically dispersed for 1 h. Subsequently, 0.5 g $MnFe_2O_4$@SiO_2 and 70 ml Diethylenetriamine (DETA) were added into to flask. The mixture refluxed with stirring for 24 h. the composite was isolated and washed with ethanol and dried in a vacuum oven at 50 °C.

Adsorption experiments

GO/DETA/$MnFe_2O_4$@SiO_2 composite was used for removal of MB dye from aqueous solutions. For this aim, different factors such as adsorbent dose, contact time, initial concentration and PH on adsorption were investigated. For doing the experiments, solution of 100 mg/l of MB was prepared in deionized water. To prepare

the experimental solutions, different amounts of composite (5–25 mg) were placed in a series of 40 ml of dye solution with different concentrations (40–120 mg/l) in 50 ml glass flasks. To study the effect of contact time of adsorbent on MB, prepared suspension solutions were stirred for 10–20 min. Beside, by using solutions of 0.01 N HCl or NaOH the effect of pH on the amount of adsorption was studied. The concentration of the MB was calculated by UV-spectrophotometer at $\lambda_{max} = 600$ nm. Equations (8) and (9) were used to calculate the amount of dye adsorbed on the adsorbent (qe in mg/g) and the percentage of solution dye removal (R in %):

$$qe = \frac{(C0 - Ce)}{M} \cdot V \tag{8}$$

$$\% R = \frac{(C0 - Ce)}{C0} \cdot 100 \tag{9}$$

where C_0 and C_e are the initial and equilibrium concentration of dye in solution (mg/l), respectively. V is the initial volume of the dye solution (l) and M is the mass of adsorbent used (g).

Data availability

All data generated or analyzed during this study are included in this published article.

Received: 4 March 2024; Accepted: 21 June 2024
Published online: 04 July 2024

References

1. Dutta, S., Gupta, B., Kumar Srivastava, S. & Kumar Gupta, A. Recent advances on the removal of dyes from wastewater using various adsorbents: A critical review. *Mater. Adv.* **2**, 4497–4531 (2021).
2. Lellis, B., Fávaro-Polonio, C. Z., Pamphile, J. A. & Polonio, J. C. Effects of textile dyes on health and the environment and bioremediation potential of living organisms. *Biotechnol. Res. Innov.* **3**, 275–290 (2019).
3. Saadat, A., Banaei, A., Sattarifar, M. & Pargolghasemi, P. Preparation 2-hydroxy-1-naphthaldehydecross-linked Fe_3O_4@chitosan-polyacrylamide nanocomposite for removal of everzol black from aqueous solutions. *Sci. Rep.* **13**, 10618 (2023).
4. Liu, N. & Wu, Y. Removal of methylene blue by electrocoagulation: A study of the effect of operational parameters and mechanism. *Ionics* **25**, 3953–3960 (2019).
5. Saufi, H. *et al.* Photocatalytic degradation of methylene blue from aqueous medium onto perlite-based geopolymer. *Int. J. Chem. Eng.* **2020**, 9498349 (2020).
6. El Ouardi, Y. *et al.* The recent progress of ion exchange for the separation of rare earths from secondary resources. *Hydrometallurgy* **2018**, 106047 (2023).
7. Cao, Y., Chen, X., Feng, Sh., Wan, Y. & Luo, J. Nanofiltration for decolorization: Membrane fabrication, applications and challenges. *Ind. Eng. Chem. Res.* **59**, 19858–19875 (2020).
8. Li, Y., Liang, Y. Q., Mao, X. M. & Li, H. Efficient removal of Cu(II) from an aqueous solution using a novel chitosan assisted EDTA-intercalated hydrotalcite-like compound composite: Preparation, characterization, and adsorption mechanism. *Chem. Eng. J.* **438**, 135531 (2022).
9. Wang, C. Adsorption of dye from wastewater by zeolites synthesized from fly ash: Kinetic and equilibrium studies. *Chin. J. Chem. Eng.* **17**, 513–521 (2009).
10. Herrera-Gonzalez, A. M., Caldera-Villalobos, M. & Pelaez-Cid, A. Adsorption of textile dyes using an activated carbon and crosslinked polyvinyl phosphonic acid composite. *J. Environ. Manag.* **234**, 237–244 (2019).
11. Banerjee, S. Adsorption characteristics of alumina nanoparticles for the removal of hazardous dye, Orange G from aqueous solutions. *Arab. J. Chem.* **12**, 5339–5354 (2019).
12. Ahmed, M. N. & Ram, R. N. Removal of basic dye from waste-water using silica as adsorbent. *Environ. Pollut.* **77**, 79–86 (1992).
13. Tahir, S. S. & Rauf, N. Removal of a cationic dye from aqueous solutions by adsorption onto bentonite clay. *Chemosphere* **63**, 1842–1848 (2006).
14. Fito, J. *et al.* Adsorption of methylene blue from textile industrial wastewater using activated carbon developed from *Rumex abyssinicus* plant. *Sci. Rep.* **13**, 5427 (2023).
15. Li, S. *et al.* Fast photocatalytic degradation of dyes using low-power laser-fabricated Cu_2O-Cu nanocomposites. *RSC Adv.* **8**, 20277–20286 (2018).
16. Weng, C. & Pan, Y. Adsorption of a cationic dye (methylene blue) onto spent activated clay. *J. Hazard Mater.* **144**, 355–362 (2007).
17. Travlou, N. A. Graphite oxide/chitosan composite for reactive dye removal. *Chem. Eng. J.* **217**, 256–265 (2013).
18. Ansari, S. A., Khan, F. & Ahmad, A. Cauliflower leave, an agricultural waste biomass adsorbent, and its application for the removal of MB dye from aqueous solution: Equilibrium, kinetics, and thermodynamic studies. *Int. J. Environ. Anal. Chem.* **2016**, 8252354 (2016).
19. Hameed, B. H. & Ahmad, A. A. Batch adsorption of methylene blue from aqueous solution by garlic peel, an agricultural waste biomass. *J. Hazard Mater.* **164**, 870–875 (2009).
20. Farooq, N. *et al.* Synthesis and characterization of clay graphene oxide iron oxide (clay/GO/Fe_2O_3) -nanocomposite for adsorptive removal of methylene blue dye from wastewater. *Inorg. Chem. Commun.* **145**, 109956 (2022).
21. Ghanbari, N. & Ghafuri, H. Design and preparation the novel polymeric layered double hydroxide nanocomposite (LDH / Polymer) as an efficient and recyclable adsorbent for the removal of methylene blue dye from water. *Environ. Technol. Innov.* **26**, 102377 (2022).
22. Cheng, T. *et al.* Synthesis of $KBiO_3$/Nano-Ag_3PO_4 composite photocatalyst and its application for degradation of organic pollutants under visible light. *Iran. J. Chem. Chem. Eng.* **41**, 1942–1960 (2022).
23. Liang, H. & Hu, X. Preparation of magnetic cellulose nanocrystal-modified diatomite for removal of methylene blue from aqueous solutions. *Iran. J. Chem. Chem. Eng.* **41**, 787–798 (2022).
24. Jawad, A. H. *et al.* Cross-Linked chitosan-glyoxal/kaolin clay composite: Parametric optimization for color removal and COD reduction of remazol brilliant blue R dye. *J. Polym. Environ.* **30**, 164–178 (2021).
25. Shi, Y. C., Wang, A. J., Wu, X. L., Chen, J. R. & Feng, J. J. Green-assembly of three-dimensional porous graphene hydrogels for efficient removal of organic dyes. *J. Colloid Interface Sci.* **484**, 254–262 (2016).
26. Huang, Z. *et al.* Differential behaviors of silver nanoparticles and silver ions towards cysteine: Bioremediation and toxicity to *Phanerochaete chrysosporium*. *Chemosphere* **203**, 199–208 (2018).
27. He, K. *et al.* Three-dimensional graphene supported catalysts for organic dyes degradation. *Appl. Catal. B: Environ.* **228**, 19–28 (2018).

28. Guo, Y., Deng, J., Zhu, J., Zhou, X. & Bai, R. Removal of mercury(ii) and methylene blue from a wastewater environment with magnetic graphene oxide: Adsorption kinetics, isotherms and mechanism. *RSC Adv.* **6**, 82523–82536 (2016).
29. Ghasemabadi, S. M., Baghdadi, M., Safari, E. & Ghazban, F. Investigation of continuous adsorption of Pb (II), As (III), Cd (II), and Cr (VI) using a mixture of magnetic graphite oxide and sand as a medium in a fixed-bed column. *J. Environ. Chem. Eng.* **6**, 4840–4849 (2018).
30. Sham, A. Y. W. & Notley, S. M. Adsorption of organic dyes from aqueous solutions using surfactant exfoliated graphene. *J. Environ. Chem. Eng.* **6**, 495–504 (2018).
31. Rouhi, M., Lakouraj, M. M., Tashakkorian, H. & Hasantabar, V. Novel carbon based bioactive nanocomposites of aniline/indole copolymer for removal of cationic dyes from aqueous solution: Kinetics and isotherms. *New J. Chem.* **43**, 2400–2410 (2019).
32. Huang, Z. *et al.* Antioxidative response of *Phanerochaete chrysosporium* against silver nanoparticle-induced toxicity and its potential mechanism. *Chemosphere* **211**, 573–583 (2018).
33. Perreault, F., Fonseca de Faria, A. & Elimelech, M. Environmental applications of graphene-based nanomaterials. *Chem. Soc. Rev.* **44**, 5861 (2015).
34. Ersan, G., Kaya, Y., ApulO, G. & Karanfil, T. Adsorption of organic contaminants by graphene nanosheets, carbon nanotubes and granular activated carbons under natural organic matter preloading conditions. *Sci. Total Environ.* **565**, 811 (2016).
35. Ersan, G., Apul, O. G., Perreault, F. & Karanfil, T. Adsorption of organic contaminants by graphene nanosheets: A review. *Water Res.* **126**, 385 (2017).
36. Thiruppathi, A. R., Sidhureddy, B., Keeler, W. & Chen, A. Facile one-pot synthesis of fluorinated graphene oxide for electrochemical sensing of heavy metal ions. *Electrochem. Commun.* **76**, 42–46 (2017).
37. Sidhureddy, B., Thiruppathi, A. R. & Chen, A. Synthesis and electrochemical study of graphene based nanomaterials for energy and environmental applications. *Chem. Commun.* **53**, 7828–7831 (2017).
38. Li, Y. *et al.* Comparative study of methylene blue dye adsorption onto activated carbon, graphene oxide, and carbon nanotubes. *Chem. Eng. Res. Des.* **91**, 361–368 (2013).
39. Fan, L. *et al.* Fabrication of novel magnetic chitosan grafted with graphene oxide to enhance adsorption properties for methyl blue. *J. Hazard. Mater.* **215**, 272–279 (2012).
40. Dai, J. *et al.* High structure stability and outstanding adsorption performance of graphene oxide aerogel supported by polyvinyl alcohol for waste water treatment. *Mater. Des.* **107**, 187–197 (2016).
41. Rashid, Z., Naeimi, H., Zarnani, A. H. & Zarnani, A. H. Fast and highly efficient purification of 6× histidine-tagged recombinant proteins by Ni-decorated $MnFe_2O_4$@SiO_2@NH_2@$_2$AB as novel and efficient affinity adsorbent magnetic nanoparticles. *RSC Adv.* **6**, 36840–36848 (2016).
42. Zinatloo-Ajabshir, S., Ghasemian, N. & Salavati-Niasari, M. Green synthesis of $Ln_2Zr_2O_7$ (Ln = Nd, Pr) ceramic nanostructures using extract of green tea via a facile route and their efficient application on propane-selective catalytic reduction of NOx process. *Ceram. Int.* **46**, 66 (2020).
43. Jeyaseelan, A., Ghfar, A., Naushad, M. & Viswanathan, N. Design and synthesis of amine functionalized graphene oxide for enhanced fluoride removal. *J. Environ. Chem. Eng.* **9**, 105384 (2021).
44. Seredych, M. & Bandosz, T. J. Mechanism of ammonia retention on graphite oxides: Role of surface chemistry and structure. *J. Phys Chem C* **111**, 15596–15604 (2007).
45. Xiao, Y. *et al.* $MnFe_2O_4$–graphene nanocomposites with enhanced performances as anode materials for Li-ion batteries. *Phys. Chem. Chem. Phys.* **15**, 3939–3945 (2013).
46. Tanhaei, B., Ayati, A., Lahtinen, M. & Sillanpaa, M. Preparation and characterization of a novel chitosan/Al_2O_3/magnetite nanoparticles composite adsorbent for kinetic, thermodynamic and isotherm studies of Methyl Orange adsorption. *Chem. Eng. J.* **259**, 1–10 (2015).
47. Travlou, N. A., Kyzas, G. Z., Lazaridis, N. K. & Deliyanni, E. A. Functionalization of graphite oxide with magnetic chitosan for the preparation of a nanocomposite dye adsorbent. *Langmuir* **29**, 1657–1668 (2013).
48. Sun, H., Cao, L. & Lu, L. Magnetite/reduced graphene oxide nanocomposites: One step solvothermal synthesis and use as a novel platform for removal of dye pollutants. *Nano Res.* **4**, 550–562 (2011).
49. Fontana, K. B. *et al.* Textile dye removal from aqueous solutions by malt bagasse: Isotherm, kinetic and thermodynamic studies. *Ecotoxicol. Environ. Saf.* **124**, 329–336 (2016).
50. Zhao, G., Li, J., Ren, X., Chen, C. & Wang, X. Few-layered graphene oxide nanosheets as superior sorbents for heavy metal ion pollution management. *Environ. Sci. Technol.* **45**, 10454–10462 (2011).
51. Wawrzkiewicz, M., Wiśniewska, M., Gun'ko, V. M. & Zarko, V. I. Adsorptive removal of acid, reactive and direct dyes from aqueous solutions and wastewater using mixed silica–alumina oxide. *Powder Technol.* **278**, 306–315 (2015).
52. Toor, M. & Jin, B. Adsorption characteristics, isotherm, kinetics, and diffusion of modified natural bentonite for removing diazo dye. *Chem. Eng. J.* **187**, 79–88 (2012).
53. Behnamfard, A. & Salarirad, M. M. Equilibrium and kinetic studies on free cyanide adsorption from aqueous solution by activated carbon. *J. Hazard. Mater.* **170**, 127–133 (2009).
54. Aboelfetoh, E. F., Gemeay, A. H. & El-Sharkawy, R. G. Effective disposal of methylene blue using green immobilized silver nanoparticles on graphene oxide and reduced graphene oxide sheets through one-pot synthesis. *Environ. Monit. Assess* **192**, 355 (2020).
55. Eltaweil, A. S., Mamdouh, I. M., Abd El-Monaem, E. M. & El-Subruiti, G. M. Highly efficient removal for methylene blue and Cu^{2+} onto UiO-66 metal–organic framework/carboxylated graphene oxide-incorporated sodium alginate beads. *ACS Omega* **6**, 23528–23541 (2021).
56. Minitha, C. R., Lalitha, M., Jeyachandran, Y. L., Senthilkumar, L. & Rajendra Kumar, R. T. Adsorption behaviour of reduced graphene oxide towards cationic and anionic dyes: Co-action of electrostatic and π – π interactions. *Mater. Chem. Phys.* **194**, 243–252 (2017).
57. Kim, H., Kang, S. O., Park, S. & Park, H. S. Adsorption isotherms and kinetics of cationic and anionic dyes on three-dimensional reduced graphene oxide macrostructure. *J. Ind. Eng. Chem.* **21**, 1191–1196 (2015).
58. Ye, S. *et al.* Biological technologies for the remediation of co-contaminated soil. *Crit. Rev. Biotechnol.* **37**, 1062–1076 (2017).
59. Li, Y. H. *et al.* Methylene, blue adsorption on graphene oxide/calcium alginate composites. *Carbohydr. Polym.* **95**, 501–507 (2013).
60. Ai, L. H. & Jiang, J. Removal of methylene blue from aqueous solution with self-assembled, cylindrical graphene-carbon nanotube hybrid. *Chem. Eng. J.* **192**, 156–163 (2012).
61. Ren, F. *et al.* Facile preparation of 3D regenerated cellulose/graphene oxide composite aerogel with high-efficiency adsorption towards methylene blue. *J. Colloid Interface Sci.* **532**, 58–67 (2018).
62. Nas, M. S. *et al.* Synthesis, characterization, kinetics and adsorption properties of Pt-Co@GO nano-adsorbent for methylene blue removal in the aquatic mediums using ultrasonic process systems. *J. Mol. Liq.* **296**, 112100 (2019).
63. Chen, P. *et al.* In situ nano-silicate functionalized graphene oxide composites to improve MB removal. *J. Taiwan Inst. Chem. Eng.* **81**, 87–94 (2017).
64. Wan, Q. *et al.* Facile and highly efficient fabrication of graphene oxide-based polymer nanocomposites through mussel-inspired chemistry and their environmental pollutant removal application. *J. Mater. Sci.* **52**, 504–518 (2017).
65. Bu, J., Yuan, L., Jiang, H. & Wang, C. Study on removal of methylene blue by condensation self-assembled graphene oxide/thiourea composite adsorbent. *Sustainability* **14**, 15290 (2022).

66. Hosseinzadeh, H. & Khoshnood, N. Removal of cationic dyes by poly(AA-co-AMPS)/ montmorillonite nanocomposite hydrogel. *Desalin. Water Treatm.* **14**, 6372–6383 (2016).
67. Zhao, J. *et al.* Synthesis of functionalized MgAl-layered double hydroxides via modified mussel inspired chemistry and their application in organic dye adsorption. *J. Colloid Interface Sci.* **505**, 168–177 (2017).
68. Guin, J. P., Bhardwaj, Y. K. & Varshney, L. Radiation crosslinked swellable ionic gels: Equilibrium and kinetic studies of basic dye adsorption. *Desalin. Water Treatm.* **57**, 4090–4099 (2016).
69. Huang, T. *et al.* Efficient removal of methylene blue from aqueous solutions using magnetic graphene oxide modified zeolite. *J. Colloid Interface Sci.* **543**, 43–51 (2019).
70. Marcano, D. C. *et al.* Improved synthesis of graphene oxide. *ACS Nano* **4**, 4806–4814 (2010).
71. Kumar, S. *et al.* Graphene oxide–$MnFe_2O_4$ magnetic nanohybrids for efficient removal of lead and arsenic from water. *ACS Appl. Mater. Interfaces* **6**, 17426–17436 (2014).

Author contributions
All authors have participated in the process of this study.

Competing interests
The authors declare no competing interests.

Additional information
Correspondence and requests for materials should be addressed to A.S.

Reprints and permissions information is available at www.nature.com/reprints.

Publisher's note Springer Nature remains neutral with regard to jurisdictional claims in published maps and institutional affiliations.